CIRP Annals - Manufacturing Technology
Volume 65, Issue 1, 2016, Pages 229-232

Acoustic emission signatures of electrical discharge machining

Andreas Klink[1], Maximilian Holsten[1], Sebastian Schneider[1], Philip Koshy[2] (1)

[1] *Laboratory for Machine Tools and Production Engineering, RWTH Aachen University, Germany*
[2] *Department of Mechanical Engineering, McMaster University, Canada*

Abstract: Relative to conventional machining processes, little is known about acoustic emission (AE) from electrical discharge machining (EDM). In light of the significant scope of AE in complementing electrical signals for the monitoring and control of EDM processes, the present research focussed on understanding AE from EDM in fundamental terms. AE waveforms are investigated in both single and sequential discharge formats with reference to pulse parameters, tool materials and dielectric media, to map AE signatures to process mechanisms. AE signals are further interpreted in terms of discharge forces, and the dynamics of gas bubbles observed through high-speed imaging of the gap.

Keywords: Electrical discharge machining (EDM), acoustic emission, material removal.

1. Introduction

The small spatio-temporal scales at which complex events transpire in electrical discharge machining (EDM) make it challenging to observe gap phenomena directly. Experimental techniques such as spectroscopy, gas chromatography and X-rays have lately facilitated new insights into process mechanisms [1]. Such techniques however focus on a particular aspect of the process, and are too sophisticated for implementation as process monitoring/control tools in a manufacturing environment.

Acoustic emission (AE) is emerging as a simple technique with the potential to not only reveal the larger picture of the EDM process state, but also adequately resolve individual discharges. The applications of AE for the in-process identification of workpiece height in wire EDM and electrode length in fast-hole EDM were reported in [2]. Recently, AE was also shown to enable the real-time assessment of gap flushing in EDM [3]; in this work, AE was observed to constitute a burst signal when discharges were initiated through the liquid medium, as opposed to their initiation through remnant gas bubbles from prior discharges. AE was thus found to encapsulate unique process information pertaining to the effectiveness with which material is removed at the scale of a single discharge. This highlights the significant scope of the AE technique in complementing the electrical waveforms that are exclusively used now for the monitoring and control of EDM machine tools.

There is a lack of fundamental knowledge on AE from EDM, due to little attention from the machining research community. Ironically, early works on the calibration and development of AE sensors have entailed electrical discharges as a source for generating AE. Likewise, electrical engineers have relied on AE for the detection of catastrophic partial discharges in power transformers. Acquiring AE from EDM is in itself simple, but interpreting it to understand source mechanisms is difficult, given that the embedded information is modulated along the signal path. The objective of the work reported in this paper was therefore to decipher AE arising from EDM in fundamental terms, with a view to mapping pertinent signatures to process mechanisms, and thereby gain new phenomenological insights into EDM.

2. Experimental

In the context of the objective above, the present investigation comprised both single and sequential discharge experiments. Single discharge experiments involved a 2 mm diameter copper wire as one of the electrodes that also functioned as a waveguide for the transmission of AE to the sensor, which had a fairly uniform frequency response in the range of 100 kHz − 900 kHz. The other electrode was a force transducer with a natural frequency of 200 kHz, which was previously found to effectively capture the evolution of force in EDM [4]. This configuration facilitated the simultaneous measurement of the force and AE signals. Discharges were realized directly on the force sensor, to exploit its entire frequency complement. Experiments were augmented by high speed imaging of the gap, which was instrumental in providing a physical interpretation of the force and AE signals in terms of the dynamics of the gas bubble.

Sequential discharge experiments used a rotating brass disk electrode with a nominal diameter of 200 mm and a thickness of 5 mm. Electrode rotation aided consistent flushing. The workpiece was of AISI 4140 steel (42CrMo4) with sectional dimensions of 18×4 mm^2, on to which the AE sensor was fastened. Experiments referred to parameters such as polarity, open circuit voltage, pulse on-time, tool material and dielectric media, the effects of which were quantified in terms of the root mean square (RMS) value.

3. Results and Discussion

AE refers to transient elastic waves generated in a material in response to dynamic mechanical loading. Propagation of these waves induces minute displacements on the surface of the material, which are transformed to a voltage waveform by the AE sensor. Considering the sequence of events in a single EDM discharge from the breakdown of the dielectric fluid to eventual material removal, AE in EDM could potentially be attributed to: the plasma channel, the gas bubble originating from the rapid vaporization of the liquid dielectric in the vicinity of the plasma channel, and the shock waves emanating from the formation, implosion and rebound of the gas bubble (Fig. 1).

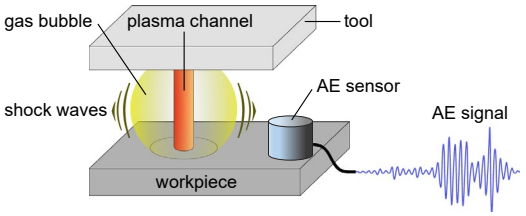

Fig. 1 Potential sources of AE in EDM.

AE from dry EDM is insignificant as compared to when using a liquid dielectric [3], which indicates the component of AE arising from the plasma channel to be relatively minor. This is supported by the observation of Garzón [4] that force waveforms from single discharges could indeed register negative values (as discussed later), when the plasma channel is still incident on the electrodes.

A simple experiment was devised to resolve the relative contributions of the remaining elements, viz. the gas bubble and the shock waves (see schematic in Fig. 2). AE sensor 1 was attached to a workpiece across which discharges were struck, such that it is subject to both the shock waves and the gas bubble. AE sensor 2 (of nominally the same characteristics as sensor 1) was attached to another workpiece of the same geometry, which was positioned in close proximity to the gap, so as to capture the influence of just the shock waves without it being in direct physical contact with the bubble. A comparison of simultaneous burst signals from the two sensors clearly shows the influence of the shock waves to be an order of magnitude smaller (Fig. 2). Swapping the sensors confirmed this to be not a sensor-related artefact. AE signal from sensor 1 that predominantly relates to the pressure within the gas bubble is henceforth of greater interest in this work.

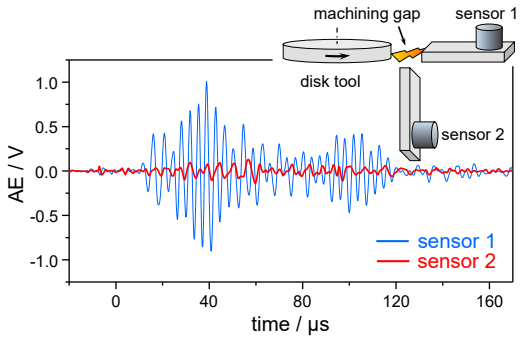

Fig. 2 AE from gas bubble and shock waves (open circuit voltage $\hat{u}_i$ 100 V, discharge current i_e 6 A, on-time t_e 50 µs, oil dielectric)

3.1 Single discharge experiments

Fig. 3A shows a typical AE burst from a single discharge. Band pass filtering the signal between 100 kHz and 400 kHz [3] significantly reduced the electromagnetic interference (EMI), a remnant of which but still remains. Although it is noise, the EMI blip usefully marks the breakdown of the dielectric fluid, saving the need to refer to the current/voltage signals. The EMI feature is followed by a time delay that refers to the time taken by the acoustic wave to reach the sensor along the length of the wire electrode. This in turn is followed by two packets of burst activity, similar to that in Fig. 2, although it is the second packet that is of a higher magnitude in this instance. In general, such variability in the relative magnitudes of the packets was characteristic of the AE signals.

The features in the AE signal can be interpreted by referring to the corresponding force signal (Fig. 3B). Relative to the on-time of 2 µs (shown as a red marker for reference), both the AE and the force signals span a time frame that is ~200 times as long. Symbols (a) to (i) shown in Fig. 3B refer to high-speed snapshots of the time evolution of the gas bubble depicted in Fig. 4.

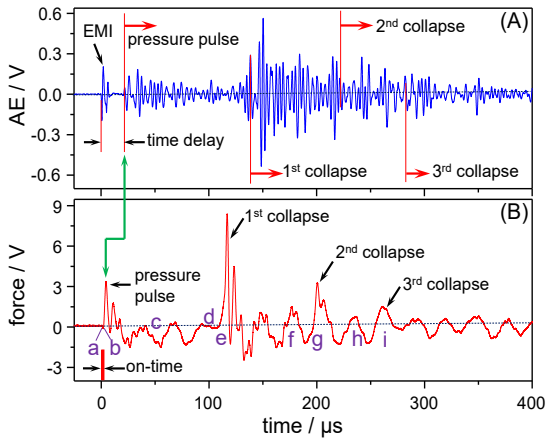

Fig. 3 Correspondence between: (A) AE, and (B) force signals ($\hat{u}_i$ 100 V, i_e 12 A, t_e 2 µs, oil dielectric)

Figs. 4a and 4b depict the inception and rapid growth of the gas bubble, which manifests a spike in the force signal that signifies the pressure within the gas bubble. The green line in Fig. 3 establishes the correspondence between the force and the AE in consideration of the time delay. By mapping the force signal to the AE signal, the pressure pulse can be seen to initiate a string of AE activity (Fig. 3A). Around the 50 µs mark, the force is rendered negative owing to over-expansion of the bubble (Fig. 4c), brought about by the inertia of the surrounding dielectric fluid. On expanding to its maximum volume, the higher hydrostatic pressure in the dielectric fluid around the bubble causes it to compress (Fig. 4d), eventually leading to its collapse at ~110 µs (Fig. 4e). The bubble collapse registers a significant increase in the force (Fig. 3B), and triggers another train of AE activity (Fig. 3A). The residual energy in the bubble results in two additional cycles of rebound (Figs. 4f & 4h) and collapse (Figs. 4g & 4i). Local maxima in the force signal between these events did not correspond to specific events in the high-speed images, and therefore appear to be related to the dynamics of the sensor.

The pressure pulse as well as the several cycles of bubble collapse can be readily identified in the force signal (Fig. 3B), but only the pressure pulse and the first collapse can be unambiguously recognised in the AE signal. It is therefore of interest to examine avenues for processing the AE signal to possibly extract additional information. Fig. 5a shows a spectrogram of the AE signal, which is a better representation of the data that brings out several features of interest. In particular, a slice of the spectrogram parallel to the time axis at a frequency of 330 kHz that corresponds to the maximum amplitude (Fig. 5b) accentuates features such as the second and third collapse, which were not as readily apparent in the AE signal (Fig. 3A).

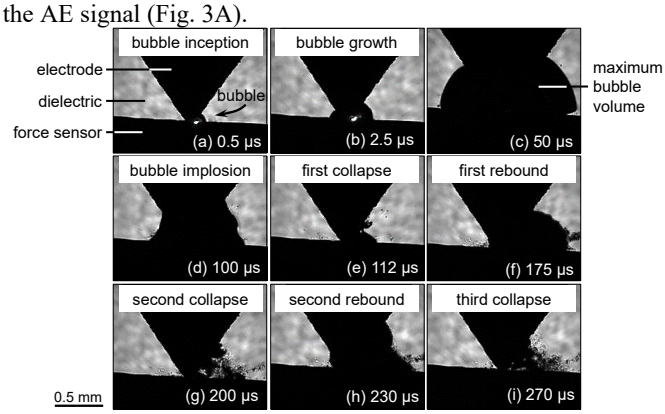

Fig. 4 Stages of bubble expansion, collapse and rebound (the wire electrode tip was shaped to be conical to localize the discharge and thus facilitate imaging).

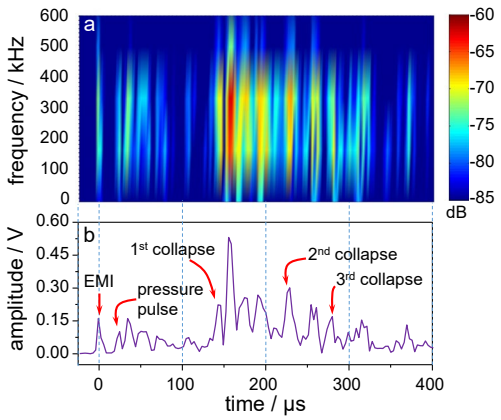

Fig. 5 (a) Spectrogram of AE burst, (b) time evolution of AE at 330 kHz.

An examination of the relationship between the peak amplitude of the force and AE signals showed a remarkable linear correlation, for values obtained over a range of current, open circuit voltage and on-time (Fig. 6). The maximum force in EDM may therefore be estimated from the AE signal on appropriate calibration. Understanding this correlation is of much practical importance considering that AE measurement is not nearly as challenging as force measurement in EDM. This information is critical for the design of micro-EDM processes that utilize slender electrodes or small diameter wires, with regard to geometric errors arising from electrode/wire deflection.

The present research underscored the implications of the bubble collapse phenomenon in EDM, the dynamics of which is influenced by the presence of a solid wall in its vicinity. Fig. 7 is a schematic representation of the several stages that constitute the first bubble collapse in a narrow channel [5], which mimics the gap space in EDM. Through the expansion phase (Fig. 7a), the potential energy of the bubble is transformed into kinetic energy of the surrounding fluid. During the subsequent bubble compression, the local kinetic energy of the fluid adjacent to the walls is lower than that near the centre of the gap. This induces fluid flow parallel to the walls and towards the bubble centre (Fig. 7b), which causes the bubble to assume an hourglass shape and eventually split (Fig. 7c). Fluid away from the walls thereafter forms microjets that penetrate the split bubbles rendering them to be ring-shaped, through the axis of which the jets impinge into either wall. The effect of jet impingement in the context of EDM was alluded to in [6] by Hockenberry and Williams five decades ago, but it seems to have garnered little traction since.

Conventionally, bubble collapse has been understood to coincide with the end of the pulse on-time, contributing to the expulsion of molten material. For instance, Tao et al [7] present a numerical simulation of bubble collapse, which elegantly captures the circumferential ridge that is so characteristic of EDM craters obtained in single discharge experiments; it should however be noted that for small pulse on-times of say 2 µs, given that the first bubble collapse does not occur until after another ~100 µs have elapsed (Fig. 4), the effect of jet impingement on material expulsion would be insignificant due to resolidification of the molten material by that time.

Interestingly, force signals from discharges corresponding to pulse on-times from 2 µs to 300 µs indicated the first collapse to occur around 100 µs, largely independent of the pulse on-time. This implies that the energy that sustains the bubble is derived from the pressure pulse that manifests during the first several µs of the bubble expansion phase, irrespective of the pulse on-time. While jet impingement during bubble collapse might therefore not contribute to ejecting molten material for low pulse on-times, depending on the thermal conductivity of the material, it may be a prominent mechanism that controls material removal efficiency as the pulse time approaches 100 µs.

Indeed, this may explain the significant increase in the measured crater depth on exceeding pulse on-times of ~100 µs, as observed by Zhang et al. [8] during their single discharge experiments involving water/oil as the working fluid. The white arrows in Figs. 8a and 8b point to initial and advanced stages respectively of microjet formation into the silhouette of the bubble before the impending second bubble collapse, even as the pulse is on (300 µs on-time). The images also show debris particles that were expelled through and out of the gas bubble into the surrounding dielectric during bubble expansion and the first bubble collapse. High-speed imaging revealed further expulsion of debris immediately following jet impingement from the second bubble collapse.

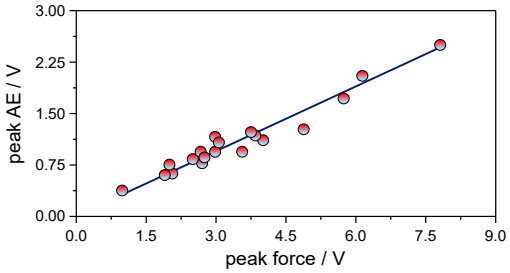

Fig. 6 Correlation of peak values from force and AE signals.

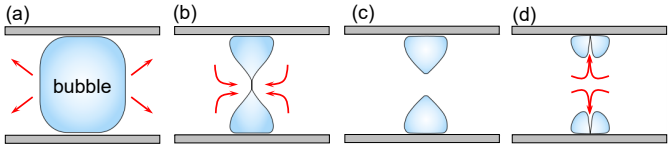

Fig. 7 Dynamics of bubble collapse in a narrow channel [5].

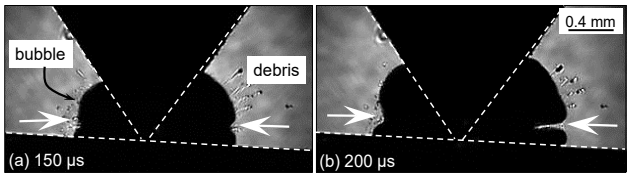

Fig. 8 Incipient formation of impinging jet.

3.2 Sequential discharge experiments

AE bursts from single discharge experiments are characterized by significant variability in terms of their magnitudes [3]. This is not an issue when averaging the AE signal over time, which fortunately is the desired format for process monitoring/control applications. A time constant of 500 ms represents a good compromise in terms of repeatability and resolution when computing the RMS values of AE from EDM.

Discharge current was shown in [3] to exhibit an optimum in the AE RMS characteristic at a current density of about 10 A/cm^2 (calculated with respect to the frontal machining area) under optimal gap flushing conditions, which is consistent with industrial practice. In contrast to this nonlinear trend, experiments in the present work indicated a linear increase in the RMS AE with an increase in the open circuit voltage (Fig. 9a). The material removal rate (MRR) in this experiment was nominally constant, indicating that the MRR does not correlate with AE RMS, when the open circuit voltage is varied. Given that an increase in the open circuit voltage does not increase the process energy (confirmed by a constant current RMS), it can be inferred that the increase in AE RMS is due to the consequent increase in the gap width. At a higher gap width, the bubble does less work against the surrounding fluid as it initially expands, and it assumes a larger volume.

More of the bubble with a higher internal pressure is thus in contact with the electrodes, resulting in a higher AE magnitude. This hypothesis was verified by comparing RMS AE when using oil and deionized water as the dielectric, for identical process parameters. AE RMS referring to deionized water was comparatively higher (Fig. 9b), which can be attributed to the kinematic viscosity of water (1 mm^2/s) being lower than that of oil (3.8 mm^2/s), which as well facilitates gas bubble expansion [4].

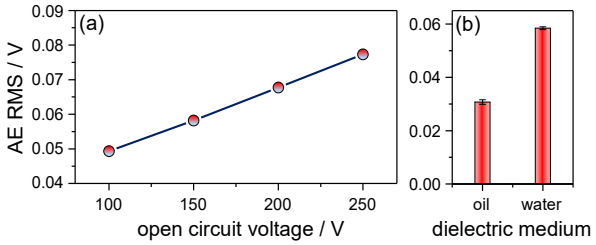

Fig. 9 Effect of: (a) open circuit voltage, and (b) dielectric medium, on RMS AE ($\hat{u}_i$ 100 V, i_e 6 A, t_e 50 µs, duty factor τ 0.5).

Fig. 10a presents the variation in AE RMS with on-time and polarity when using oil dielectric. While the AE RMS was comparable for pulse on-times in the range of 5 µs − 20 µs, a tool-negative polarity referred to higher values for lower on-times, and vice versa. This aligns with the well-known effect of these parameters on the MRR in EDM [1], which is the basis for commonly employing tool-positive polarity in sinking EDM, except for when using pulse on-times of just several µs.

The decreasing trend of AE RMS with on-time for either polarity is due to decreasing discharge frequency, which reduces the contribution to the AE RMS from the pressure pulse that follows dielectric breakdown. The reason for the crossover in the characteristics is however not as readily evident. The difference in the removal between the anode and the cathode has conventionally been attributed to a difference in the mobility of ions and electrons: a concept that has recently been called into question [9]. Indeed, should the mobility hypothesis be true, the energy partition between the electrodes should be dependent on the pulse on-time over the range indicated, which contradicts experimental observations [1].

Kunieda and Kobayashi [10] have offered an alternate explanation that attributes the polarity effect to the pyrolytic carbon deposited on the anode surface when the on-time exceeds ~20 µs. AE RMS experiments repeated in water (as opposed to oil) exhibited no crossover as in Fig. 10a, with the tool-negative polarity referring to higher values for the entire range of pulse on-time; this indicated the crossover to be related to carbon deposition. Further experiments involving different tool materials indicated the AE RMS to decrease with an increase in thermal conductivity λ (Fig. 10b). In light of the results above and considering that AE in EDM essentially represents energy within the bubble, which is basically the difference between the input energy and the energy lost to the electrodes, the results in Fig. 10a may be explained in reference to the energy partition to the anode and the cathode, and the difference in the energy conducted through the electrodes.

When the tool is negatively polarized, more energy is partitioned to the steel workpiece (anode); only a small proportion of this energy is conducted away due to the relatively low thermal conductivity of 4140 steel (43 W/mK), resulting in more energy available within the bubble that translates into a higher RMS AE. For tool positive polarity, the higher energy partition to the tool is offset by the higher thermal conductivity of the brass tool (120 W/mK) relative to the steel workpiece, which leaves less energy in the bubble and hence a lower AE RMS. This explains the higher AE RMS for tool negative polarity at the lower end of pulse on-time. For pulse on-time of ~20 µs and higher, when the tool polarity is positive, the deposition of the carbonaceous layer on the tool represents a thermal barrier which inhibits energy transfer to the tool; this results in more energy in the bubble, which corresponds to a higher AE RMS relative to the tool-negative polarity.

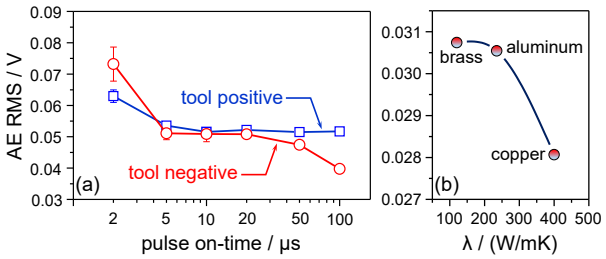

Fig. 10 Effect of: (a) on-time and polarity, and (b) thermal conductivity, on RMS AE ($\hat{u}_i$ 100 V, i_e 6 A, t_e 50 µs, τ 0.5).

4. Conclusions

Features in burst AE from single discharges were elucidated by simultaneous force measurement and high-speed imaging. The AE signal was shown to essentially reflect the energy available within the gas bubble, and comprise features pertaining to the pressure pulse from the rapid expansion of the gas bubble, followed by several collapse and rebound cycles. Microjet impingement on the electrode surfaces was identified to contribute to material removal for discharges with pulse on-time approaching ~100 µs and higher. Sequential discharge experiments were found to lend credence to the theory invoking the role of pyrolytic carbon to explain the effects of polarity and on-time in EDM. The present work highlights the significant potential of AE in enabling further unique insights into EDM.

Acknowledgements

A fellowship to P. Koshy from the Humboldt Foundation is acknowledged. Authors thank the German Research Foundation (DFG) for funding the Collaborative Research Centre SFB / TRR 136 “Function Oriented Manufacturing Based on Characteristic Process Signatures,” project F02.

References

1. Kunieda M, Lauwers B, Rajurkar KP, Schumacher BM (2005) Advancing EDM through Fundamental Insight into the Process. *CIRP Annals–Manufacturing Technology* 54:64-87.
2. Smith C, Koshy P (2013) Applications of Acoustic Mapping in Electrical Discharge Machining. *CIRP Annals–Manufacturing Technology* 62:171–174.
3. Goodlet A, Koshy P (2015) Real-Time Evaluation of Gap Flushing in Electrical Discharge Machining. *CIRP Annals–Manufacturing Technology* 64:241-244.
4. Garzón M (2013) Analysis of Discharge Forces in Sinking EDM with High Aspect Ratio Electrodes. PhD Thesis, RWTH Aachen University.
5. Mousavi R, Ahmadi G (2008) Intensification of the Near Wall Collapsing Bubble Induced Jet Using an Opposite Secondary Wall. *Journal of Fluid Science and Technology* 3:207-218.
6. Hockenberry TO, Williams EM (1967) Dynamic Evolution of Events Accompanying the Low Voltage Discharges Employed in EDM. *IEEE Transactions on Industry and General Applications* 3:302–309.
7. Tao J, Ni J, Shih AJ (2012) Modeling of Anode Crater Formation in Electrical Discharge Machining. *Journal of Manufacturing Science and Engineering* 134:011002-011002-11.
8. Zhang Y, Liu Y, Shen Y, Ji R, Li Z, Zheng C (2014) Investigation on the Influence of Dielectric on the Material Removal Characteristics of EDM. *Journal of Materials Processing Technology* 214:1052-1061.
9. Hinduja S, Kunieda M (2013) Modelling of ECM and EDM processes. *CIRP Annals–Manufacturing Technology* 62:775-797.
10. Kunieda M, Kobayashi T (2004) Clarifying Mechanism of Determining Tool Electrode Wear Ratio in EDM using Spectroscopic Measurement of Vapor Density. *Journal of Materials Processing Technology* 149:284-288.